



**HAL**  
open science

# From Ni–P Metastable Alloy Nanoparticles to Bulk Submicrometer Grain-Sized MMCs with Tunable Mechanical and Magnetic Properties

Mohamed Ali Bousnina, Frédéric Schoenstein, Silvana Mercone, Nouredine Jouini

► **To cite this version:**

Mohamed Ali Bousnina, Frédéric Schoenstein, Silvana Mercone, Nouredine Jouini. From Ni–P Metastable Alloy Nanoparticles to Bulk Submicrometer Grain-Sized MMCs with Tunable Mechanical and Magnetic Properties. *Metals*, 2020, 10 (1), pp.112. 10.3390/met10010112 . hal-04188672

**HAL Id: hal-04188672**

**<https://hal.science/hal-04188672>**

Submitted on 26 Aug 2023

**HAL** is a multi-disciplinary open access archive for the deposit and dissemination of scientific research documents, whether they are published or not. The documents may come from teaching and research institutions in France or abroad, or from public or private research centers.

L'archive ouverte pluridisciplinaire **HAL**, est destinée au dépôt et à la diffusion de documents scientifiques de niveau recherche, publiés ou non, émanant des établissements d'enseignement et de recherche français ou étrangers, des laboratoires publics ou privés.

Article

# From Ni–P Metastable Alloy Nanoparticles to Bulk Submicrometer Grain-Sized MMCs with Tunable Mechanical and Magnetic Properties

Mohamed Ali Bousnina, Frédéric Schoenstein , Silvana Mercone  and Noureddine Jouini \* 

Laboratoire des Sciences des Procédés et des Matériaux, CNRS, UPR 3407, Université Paris 13, Sorbonne Paris Cité, 99 avenue Jean Baptiste Clément, F-93430 Villetaneuse, France; medalibousnina@yahoo.fr (M.A.B.); frederic.schoenstein@univ-paris13.fr (F.S.); silvana.mercone@univ-paris13.fr (S.M.)

\* Correspondence: jouini@univ-paris13.fr; Tel.: +33-1-49-40-34-35

Received: 4 December 2019; Accepted: 8 January 2020; Published: 11 January 2020



**Abstract:** In this study, submicrometer grain-sized metal matrix composites (MMCs) based on nickel were elaborated via a bottom-up strategy combining the polyol process and a non-conventional heat treatment route. First, four sets of nano-sized Ni–P metastable alloy nanopowders with an average particle size centered at 50, 100, 130, and 220 nm were prepared by the polyol process modified by the addition of hypophosphite (strong reducing agent) and heterogeneous nucleation using silver nitrate and platinum salt (nucleating agents). The heat treatment step was realized by reactive spark plasma sintering (R-SPS) at identical heat treatment conditions (600 °C, 53 MPa, and 10 min as holding time). R-SPS transformed the Ni–P metastable alloys into bulk submicrometer grain-sized MMCs with Ni as the matrix and Ni<sub>3</sub>P as the reinforcement. Mechanical and magnetic properties of the four MMC samples were found to be closely related to the grain size of the Ni matrix, which varied from 247 to 638 nm. Yield stress, maximum stress, and coercive field increased when the grain size decreased, while plastic strain and magnetization saturation decreased. The reinforcement Ni<sub>3</sub>P phase enhanced the mechanical characteristics of the composite. Crossover behavior was observed at around 350 nm Ni grain size, where a ductile and soft magnetic composite was tuned into a hard mechanical and semi-hard magnetic one.

**Keywords:** metal matrix composite; metastable Ni–P alloy; submicrometer grain-sized materials; bottom-up strategy; mechanical and magnetic properties

## 1. Introduction

Spark plasma sintering (SPS) has emerged as a promising nonconventional consolidation process. Indeed, SPS is characterized by a specific heat treatment in comparison with powder metallurgy methods; a high sintering rate and a local high temperature generated by spark discharges leading to a very low consolidation time. This enables a dense consolidation without excessive grain growth. Thus, when the starting material is in the form of a nanopowder, the as-obtained bulk material is nanostructured or submicrometer grain-sized and shows structural and physical properties closely governed by its fine microstructure [1].

Besides these advantages, several recent works have shown that SPS can also be used as a reactive process to elaborate nanostructured or submicrometer grain-sized materials starting from raw reactants [2–5]. In this process, called reactive SPS (R-SPS), synthesis and densification are achieved in a single step. For instance, Patissier et al. reported the synthesis of LaFe<sub>13-x</sub>Si<sub>x</sub> magnetocaloric compounds by the R-SPS process starting from a mixture of ball-milled LaSi, Fe, and Si elements [6].

In this context, we have undertaken a general project to elaborate metal matrix composites (MMCs) based on nickel. In the first step, metastable Ni–P alloys in the form of nanoparticles were elaborated

by the polyol process. These particles had the fcc nickel structure with phosphorus inserted inside [7]. In the second step, the R-SPS process transformed these metastable alloys into bulk submicrometer grain-sized MMCs, where the matrix was composed of nickel and Ni<sub>3</sub>P was the reinforcement phase. In the first part of this work [8], we reported on the influence of two sintering parameters, namely, temperature and holding time, on the mechanical and magnetic properties of MMC Ni–Ni<sub>3</sub>P obtained from nanoparticles of metastable Ni–P alloys with a 100 nm diameter. We report here in the second part on the influence of the starting nanoparticle size of metastable Ni–P alloys on the properties of the obtained submicrometer grain-sized MMCs while using identical sintering conditions. Both parts show that some parameters, such as holding time and Ni–P nanoparticle size, play a key role in the large-scale tuning of the properties of such obtained materials.

## 2. Materials and Methods

### 2.1. Synthesis

The experimental protocol adopted to elaborate the Ni–P powders has been described in a previous work [9]. This synthesis protocol allowed us to elaborate particles with sizes ranging from 50 to 130 nm. In the present work, we modified this protocol by adding a certain amount of silver nitrate as nucleating agents ( $[AgNO_3] = 2 \times 10^{-5}$ ) in order to obtain larger particles, namely 220 nm in diameter.

Prior to the R-SPS process, the Ni–P powder was initially heated under hydrogen at 300 °C for 1 h in order to clear them from organic molecules and to thermally reduce all traces of nickel oxide present on the surface of the particles.

The R-SPS experiments were realized according to the following process: 2 g of the Ni–P nanopowders was versed in a cylindrical graphite matrix (internal diameter of 10 mm). After establishing a primary vacuum in the apparatus, uniaxial pressure was firstly applied on the graphite die containing the powder. Its value was increased up to 53 MPa in 1 min and then the heating started while maintaining this pressure. The heating rate was 60 °C min<sup>-1</sup> and the holding time was 10 min at 600 °C. Under these conditions, the as-obtained specimens presented a height of about 3 mm.

### 2.2. Characterization Techniques

X-ray diffraction (XRD) patterns of the synthesized powders and the bulk samples were obtained using an INEL EQUINOX 1000 diffractometer (INEL, Artenay, France) operating with CuK $\alpha$  radiation ( $\lambda = 1.5406 \text{ \AA}$ ). The existing phases were determined using the International Centre for Diffraction Data-Powder Diffraction Files 2 (ICDD PDF2) database. The lattice parameters and the average crystallite sizes were calculated with the FullProf program (Version 2006) [10] using the Rietveld method [11]. The particle size, the morphology, and the microstructure of the consolidated samples were studied using a JEOL-2011 transmission electron microscope (TEM, JEOL, Tokyo, Japan) operating at 200 kV. Microstructure examination of fracture surfaces was carried out using Field Emission Gun Scanning Electron Microscopy (FEG-SEM; Ziess, Oberkochen, Deutschland). The grain size of Nickel and Ni<sub>3</sub>P was determined by a statistical study of 200 particles using the Image Tool program (Free software, Version 2, University of Texas Health Science Center, San Antonio, TX, USA). The phosphorus content in the samples was determined by inductively coupled plasma (ICP) measurements. The SPS process of the powders was accomplished with an SPS-515S SYNTEX apparatus (Fuji Electric Industrial Co., Osaka, Japan). The densities of the consolidated samples were measured by the Archimedes method using 2-propanol as a measuring liquid (0.786 density at 25 °C). Compressive tests of specimens with dimensions of 1.5 mm  $\times$  1.5 mm  $\times$  2.4 mm were conducted at room temperature (RT) using a homemade micro-sample testing machine with a load cell of 5 kN maximum capacities and a strain rate of about  $3.5 \times 10^{-3} \text{ s}^{-1}$ . Microhardness measurements were conducted on the perpendicular plane to the pressing direction using a Duramin 20 Vickers device (Struers S.A.S., Champigny sur Marne, France) with a test force of 1.916 N for 10 s. Multiple measurements (20) were carried and the average

value was taken to reduce errors. The magnetic properties of samples were measured using a Quantum Design MPMS 3 (Magnetic Property Measurement System) magnetometer (Quantum Design Inc., San Diego, CA, USA). Magnetization as a function of the magnetic field was collected in the magnetic field range of  $[-3 \text{ T}, +3 \text{ T}]$  at 10 and 300 K.

### 3. Results

#### 3.1. X-Ray Diffraction and TEM Characterizations

The XRD patterns of as-prepared powders presented the symmetry of the pure nickel (Figure 1). The best refinements of these diffractograms were obtained using a cubic face-centered crystal symmetry with almost similar lattice parameter ( $a = 3.523 \text{ \AA}$ ) to that of pure Ni (PDF card No. 04-0850,  $a = 3.524 \text{ \AA}$ ), despite the presence of a significant amount of P (2%–4% by weight) [7,8]. This P composition is significantly higher than that reported in the stable equilibrium diagram of the Ni–P system wherein the solid solution Ni–P is very limited in phosphorus content, not exceeding 0.17% by weight [12]. Thus, the as-obtained alloys can be considered as metastable phases. TEM studies have shown that the particles obtained are equiaxed, with size varying in the range of 50–220 nm (Table 1) (see Supplementary Material S1).

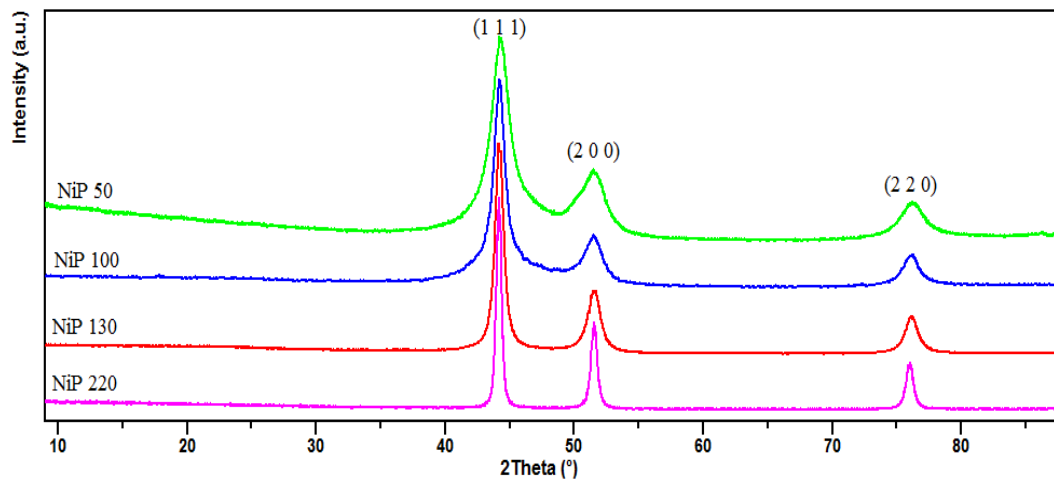


**Figure 1.** X-ray diffraction (XRD) patterns of starting Ni-P powder.

**Table 1.** Summary results of densified Ni–P samples: particle size of starting Ni–P powder was determined by transmission electron microscope (TEM), crystallite size by the Rietveld method of X-ray diffraction (XRD) patterns, grain size by TEM, the % mass of P by inductively coupled plasma (ICP), and Ni and Ni<sub>3</sub>P phases by the Rietveld method. SPS, spark plasma sintering.

Samples	Particle Size of Ni-P Powder (nm)	Crystallite Size of Ni (nm)	Crystallite Size of Ni <sub>3</sub> P (nm)	Grain Size of Ni (nm)	Grain Size of Ni <sub>3</sub> P (nm)	% Mass P (ICP)	% Mass Ni <sub>3</sub> P (Rietveld)
NiP50SPS	50 ± 9	38.2	10.8	247 ± 39	97 ± 29	4.16	9.84
NiP100SPS	100 ± 18	49.9	14.5	330 ± 21	134 ± 28	4.01	9.40
NiP130SPS	130 ± 19	54.8	16.2	383 ± 27	141 ± 28	3.72	7.19
NiP220SPS	220 ± 12	81.1	20.6	638 ± 80	187 ± 33	2.22	4.97

The XRD patterns of densified samples obtained by the R-SPS process showed, besides intense peaks of Ni, the presence of low-intensity peaks (Figure 2). According to the X-ray diffraction database, these peaks can be attributed to Ni<sub>3</sub>P phase (PDF Card No. 34-0501). This phase was formed during the SPS process and derived from the use of sodium hypophosphite in the synthesis process [6]. Actually, SPS acted as a reactive process and transformed the metastable alloys into bulk submicrometer grain-sized MMCs, where the matrix was composed of nickel and Ni<sub>3</sub>P was the reinforcement phase

formed during sintering. The mechanism of this phase apparition assumed the diffusion of phosphorus from the inside of the initial nanoparticles to the grain boundaries, where nucleation and growth of  $\text{Ni}_3\text{P}$  nanoparticles occurred. Grain growth during heat treatment by SPS was accompanied by narrowing peaks observed on XRD patterns.

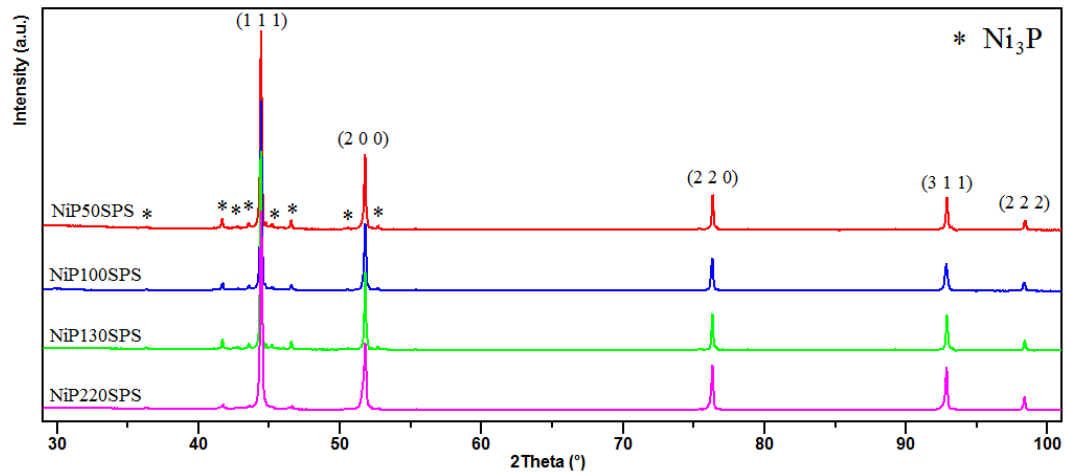


**Figure 2.** XRD patterns of metal matrix composites (MMCs) based on Ni-densified Ni-P samples obtained by reactive spark plasma sintering (SPS) from different particle sizes of nanopowders.

The weight percentages and the crystallite size of both phases were determined using the Fullprof program based on the Rietveld method (Table 1). The weight percentages of  $\text{Ni}_3\text{P}$  phases varied from 5% to 10%.

TEM investigations of the microstructure of the bulk samples and the grain size distributions determined by TEM are presented in Figure 3. It was found that the mean grain size values for nickel depended on the size of the starting Ni–P alloy nanoparticles. The larger the size of the initial particles of Ni–P alloys, the larger the grain size of Ni present in the MMC materials—about 3–5 times larger than the mean particle sizes in the initial powders (see Table 1). However, the grain growth was more important when the starting nanoparticle size was lower, indicating that the high-temperature consolidation (600 °C) resulted in grain coarsening, in agreement with previous reports [13,14]. It should be noted that the grain size of  $\text{Ni}_3\text{P}$  nanoparticles increased concomitantly with that of Ni, which was the matrix phase.

The SPS process induced a significant change in the morphology. We could note in the two as-processed material grain types. The major one consisted of polygonal grains with mean sizes varying from 247 to 638 nm depending on the size of the starting particles. Obviously, these grains corresponded to the Ni compound. The minor one corresponded to equiaxial nanoparticles, with sizes not exceeding 187 nm. Some were located at triple junctions of Ni grains; others were located inside or on the grain boundaries of the nickel. This organization was recently reported by Prasad et al. in an Ni–P system obtained by electrodeposition [15]. Given their small size, these nanoparticles can match the  $\text{Ni}_3\text{P}$  phase that was formed during the R-SPS step. This result was confirmed in a previous work by electron energy loss spectroscopy (EELS) analysis [7].

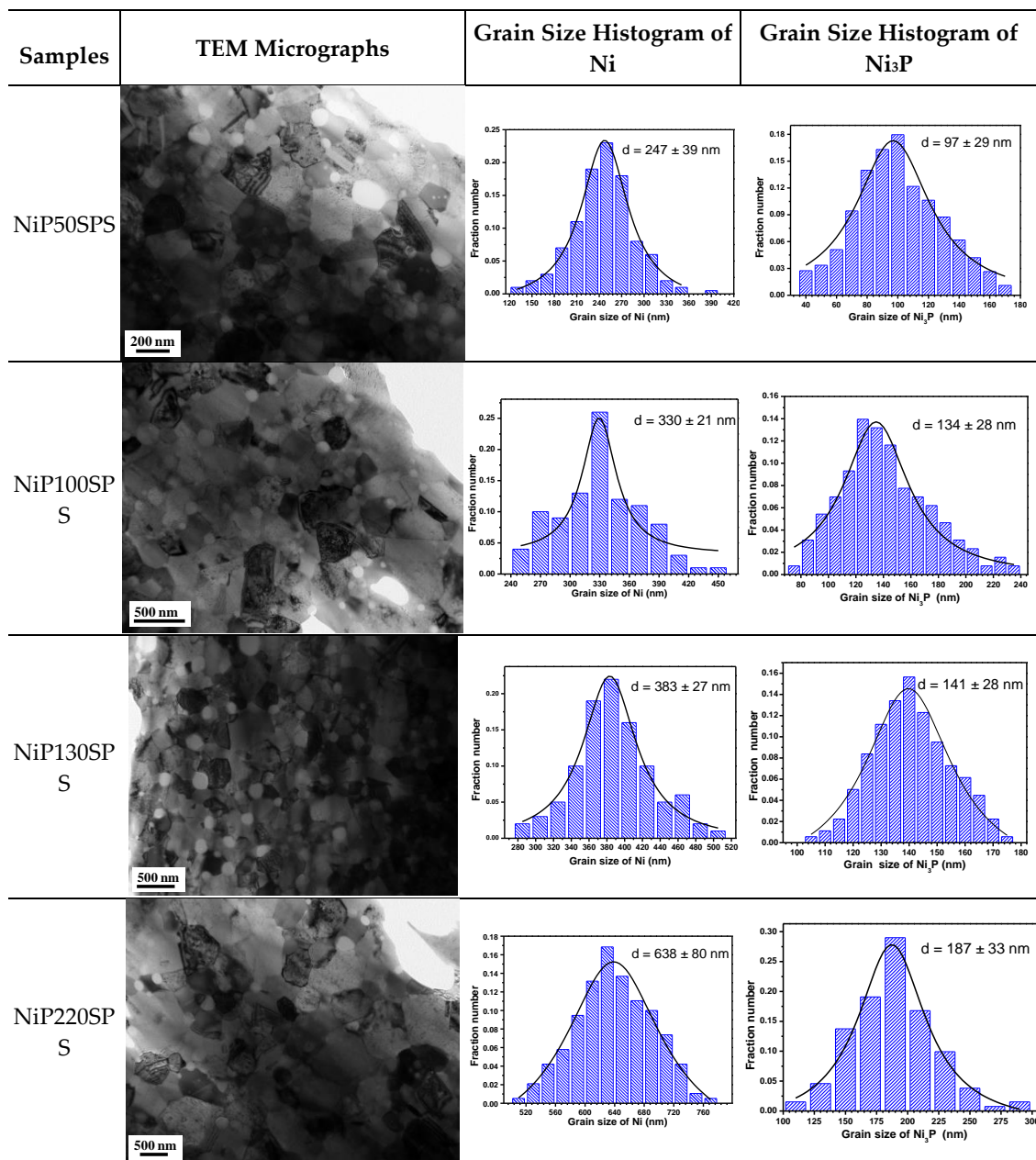


**Figure 3.** Transmission electron microscope (TEM) observations submicrometer grain-sized samples and grain size histogram of Ni and Ni<sub>3</sub>P.

The crystallite size of both phases is given in Table 1. The variation of the grain size of nickel and Ni<sub>3</sub>P as a function of crystallite size is illustrated in Figure 4. Regardless of the particle size of the starting powders, an almost linear correlation was observed between the crystallite size and the grain size for both phases. Indeed, the grain size increased as the crystallite size increased.

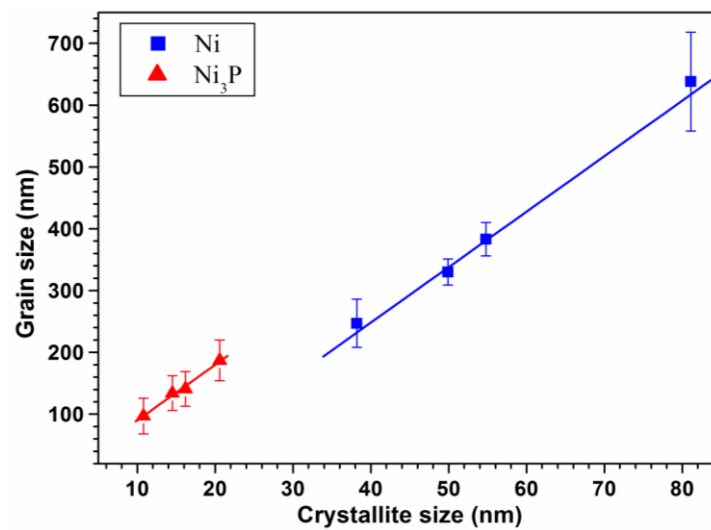


**Figure 4.** Variation of grain size of Ni (■) and Ni<sub>3</sub>P (▲) as a function of crystallite size of MMCs.

Table 2 shows the grain size of Ni and Ni<sub>3</sub>P, the relative density, and the microhardness (Hv) values for the sintered samples. It was found that the relative density increased linearly as a function of the grain size within the SPS experimental conditions used in this work (53 MPa, 10 min, and 600 °C). The samples do not reach a fully dense consolidation. Indeed, a residual porosity remains for all samples; it increases when the grain size decreases and varies between 5.5% and 2.2%.

**Table 2.** Summary of grain sizes of Ni and Ni<sub>3</sub>P and values of relative densities and microhardness (Hv) for Ni–P samples.

Samples	Grain Size of Ni (nm)	Grain Size of Ni <sub>3</sub> P (nm)	Relative Densities (%)	Hv
NiP50SPS	247 ± 39	97 ± 29	94.5	522 ± 4
NiP100SPS	330 ± 21	134 ± 28	95.6	593 ± 5
NiP130SPS	383 ± 27	141 ± 28	96.2	615 ± 5
NiP220SPS	638 ± 80	187 ± 33	97.8	355 ± 6

The Vickers microhardness increased gradually, reaching a maximum of Hv = 615 for a Ni grain size of 383 nm and a relative density of 96.2%. For an Ni grain size higher than 383 nm, a dramatic decrease of the microhardness was observed despite a very low porosity (2.2%).

### 3.2. Compressive Test

Figure 5 shows the true stress versus true strain curves of the MMCs. The mechanical properties of these samples are summarized in Table 3.

It appears that the mechanical behavior of densified samples was governed by grain growth. Indeed, it can be seen that the MMC with a large grain size higher than 0.5 μm (NiP220SPS) presented mechanical characteristics very close to those of bulk nickel, namely, low yield strength (621 MPa), low maximum stress (894 MPa), and large ductile plateau with a plastic strain of 36.8%. It had a relatively long hardening, followed by a progressive softening leading to rupture.

This behavior did not occur for samples with a lower grain size. Indeed, when the grain size decreased, the mechanical characteristics evolved toward those of a brittle material, the plastic strain decreased down to 2.6%, and the yield strength and maximum stress increased up to 1408 and 1638 MPa, respectively.

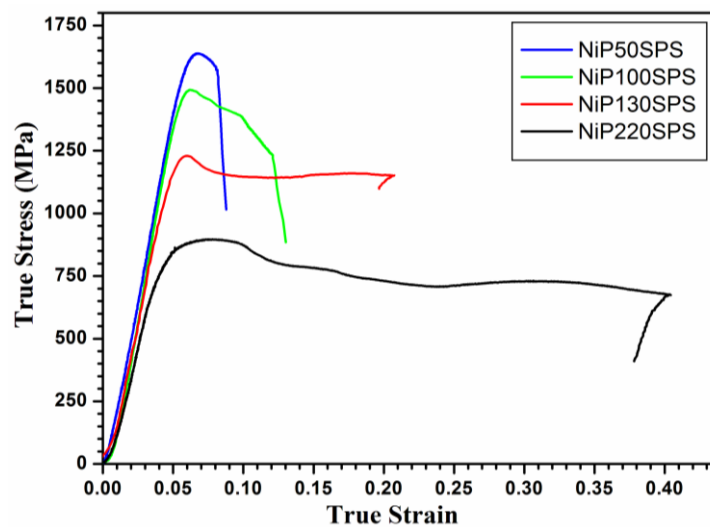


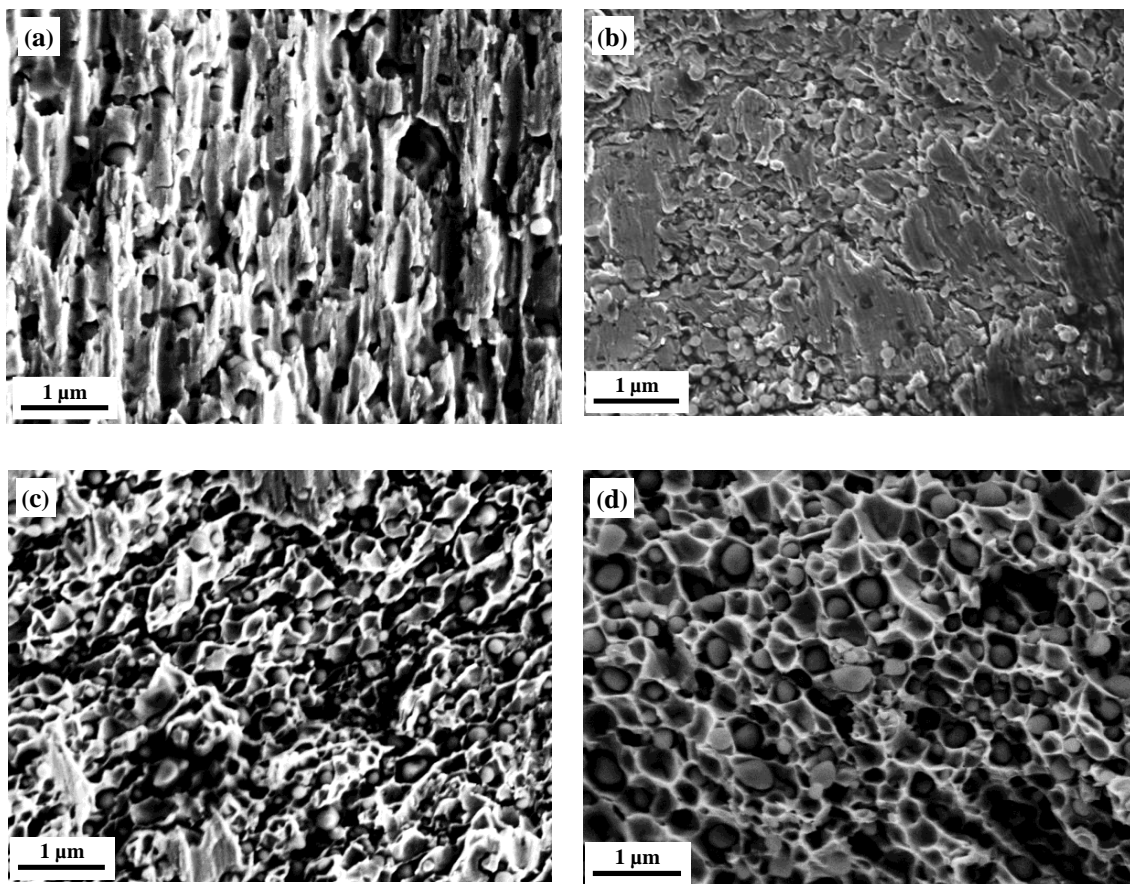
Figure 5. True stress vs. true strain curves obtained from compression test of MMCs.

Table 3. Mechanical characteristics of the metal matrix composites (MMCs).

Samples	Grain Size of Ni (nm)	Yield Strength (MPa)	Maximum Stress (MPa)	Plastic Strain (%)
NiP50SPS	247 ± 39	1408	1638	2.9
NiP100SPS	330 ± 21	1190	1493	4.7
NiP130SPS	383 ± 27	968	1229	16.4
NiP220SPS	638 ± 80	621	894	36.8

### 3.3. Fracture Behaviors

The fracture surfaces of the submicrometer grain-sized samples after compression tests at room temperature (RT) were observed by FEG-SEM (Figure 6). The fracture surfaces showed that the behavior of these materials varied between that of a hard and brittle material (NiP50SPS) and that of a ductile and low-strength material (NiP220SPS). Indeed, for the NiP50SPS sample, the rupture was fragile, characterized by a shiny surface with rivers and ridges, on which one can notice the presence of grains (Figure 6a). On the contrary, the fracture was essentially ductile in the case of the NiP220SPS sample, characterized by the presence of cupules and cones (Figure 6d). The transition between brittle and ductile failure was not sudden; in fact, the intermediate samples NiP100SPS and NiP130SPS (Figure 6b,c) present both fragments with ductile fracture along with fragments with a brittle one.



**Figure 6.** FEG-SEM observation of the fracture surfaces of submicrometer grain-sized samples: (a) NiP50SPS, (b) NiP100SPS, (c) NiP130SPS, and (d) NiP220SPS.

### 3.4. Magnetic Properties

The magnetic behavior of MMC samples was studied by measuring the static magnetization as a function of the magnetic field at two different temperatures: 10 and 300 K. Figure 7a,b show the hysteresis loops of all the samples at 10 and 300 K, respectively. Table 4 reports the average grain and crystallite size together with the magnetic characteristics of these materials (coercive field, magnetization at remanence, and saturation). It should be noted that the magnetic characteristics of NiP100SPS obtained in the present work are, within the experimental error, in good agreement with our previous results [8].

**Table 4.** Magnetic characteristics of materials produced by reactive SPS (R-SPS).

Samples	Grain Size of Nickel (nm)	Crystallite Size of Nickel (nm)	Hc (Oe)		Mr (emu g <sup>-1</sup> )		Ms (emu g <sup>-1</sup> )	
			10 K	300 K	10 K	300 K	10 K	300 K
NiP50SPS	247 ± 39	38.2	86.7	26.3	2.9	0.96	43.3	41.3
NiP100SPS	330 ± 21	49.9	55.4	5.2	2.6	0.33	48.1	46.2
NiP130SPS	383 ± 27	54.8	40.6	1.8	2.1	0.15	50.2	48.1
NiP220SPS	638 ± 80	81.8	22.8	0.6	0.9	0.03	54.7	52.3

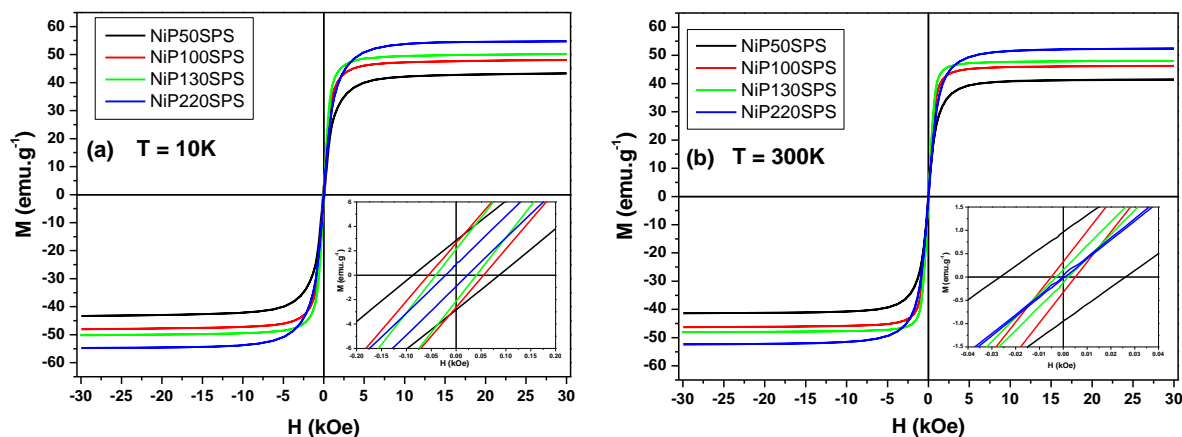


**Figure 7.** Hysteresis loops at 10 (a) and 300 K (b) of materials produced by reactive SPS (R-SPS) from various particle sizes of Ni-P nanopowders.

Both at low and room temperatures, the samples presented a ferromagnetic behavior, showing the usual decrease of the coercive field and the saturation magnetization when the temperature increased. This allowed affirming that, no matter the grain size, the magnetic properties of the MMCs were mainly driven by the ferromagnetic Ni matrix and not the paramagnetic Ni<sub>3</sub>P included phase.

Table 4 illustrates the variation of H<sub>c</sub> and M<sub>s</sub> as a function of the grain and crystallite size of nickel, confirming that the submicron characteristic also governed the magnetic properties of the prepared materials. The coercive field increased when the grain and crystallite size of nickel decreased: the higher coercive field was obtained for the MMC showing the lowest grain size of nickel (247 nm). In this latter case, we observed a coercive field almost twice that of the one observed in the agglomerate bulk nickel materials obtained by conventional compaction at a similar temperature (52 Oe) [16]. Conversely, magnetization at the saturation value increased when the grain size increased. However, it is worth noting that all M<sub>s</sub> were only slightly reduced compared with that of the bulk nickel (55 emu g<sup>-1</sup>) [17], confirming the good quality of our Ni-based sintered materials. The small difference can be attributed both to (i) the presence of Ni<sub>3</sub>P, which has a paramagnetic behavior; and (ii) the variation of grain and crystallite sizes of Ni, with this latter parameter appearing to be the most important one, as discussed in Section 4.

#### 4. Discussion

Relatively dense submicrometer grain-sized MMC Ni-P alloys have attracted much scientific and technical attention because of their excellent functional properties compared with conventional polycrystalline materials [18–20]. The mechanical properties, owing to their fine grain size, are characterized by high strength and relatively high ductility [21,22]. Their corrosion resistance, high hardness, and wear resistance as well as electrical, magnetic, and catalytic properties have made these alloys excellent candidates for use in electric motors, chemical applications, and several others areas [20,23,24].

These alloys can be prepared by two principal processes: electroless or electrodeposition methods. Both methods require the use of a complex bath composed of several salts, each having a specific role (reducing agent (generally, the hypophosphite anion), complexing agent, pH buffers, accelerators, stabilizers, and wetting agents) [25]. The alloys elaborated by the deposition methods commonly come in film form. Thus, an additional heat treatment is needed to improve the crystallinity and mechanical properties of these materials. This step confers to these films a very high hardness and can be used as wear-resistant coatings. However, these materials are subject to severe brittleness, which makes their workability not an easy task.

In the present work, along with our previous works [7–9,26], we proposed a novel method to elaborate Ni-P alloys in the form of nanoparticles instead of films. This method requires a simplified

bath only constituted of polyol, in which the hypophosphite is added in order to enhance the reducing power of the medium. The obtained Ni–P nanoparticles are spherical with well-controlled size and polycrystalline structure. Unlike the Ni–P alloys prepared by electroless or electrodeposition [22,27,28], nanoparticles prepared by the polyol process show high crystalline quality. While electroless and electrodeposition processes enable the elaboration of films, our bottom-up strategy using the R-SPS process and starting from nanopowders of Ni–P alloys leads to bulk submicrometer grain-sized MMCs, which are characterized by an Ni matrix and Ni<sub>3</sub>P inclusions as a reinforcement material (wt % of 5–10%). This is coherent with our previous results obtained for 100 nm Ni–P alloys [8].

In the work of [8], by varying the heat treatment conditions (temperature, time, and pressure), various MMC materials were obtained with a tunable grain size, varying in the ranges of 179–560 and 101–223 nm for Ni and Ni<sub>3</sub>P, respectively.

In the present work, the R-SPS conditions were fixed (temperature of 600 °C, holding time of 10 min, and pressure of 53 MPa), while the starting nanoparticle size varied from 50 to 220 nm. This resulted in MMCs that also had a tunable grain size between 247 and 638 nm for Ni and between 97 and 187 nm for Ni<sub>3</sub>P. A relationship exists between the starting nanoparticle size of Ni–P alloys and the grain size of the Ni in the as-obtained MMCs; the larger the size of the starting Ni–P alloy particles, the larger the size of Ni grains in MMCs.

As can be seen, the two approaches led to almost identical grain size ranges for both components.

The grain sizes inferred from TEM images were significantly higher than the crystallite sizes inferred from XRD analyses. Crystallites are in fact the smallest domain inside the grain, which scatter X-rays coherently. This coherency breaks even if the crystallites have very small misorientation (1°–2°). Thus, the crystallites inside of the grain can be considered as subgrains [29,30]. More interesting to note, the grain size varied linearly with the crystallite size; it increased when the crystallite size increased. Furthermore, for Ni grains, the grain size/crystallite size ratio varied in a narrow range: 6.5–8, similar to that observed in the work of [8]. Accordingly, the mechanical and magnetic properties of these materials can either be correlated to the submicrometer microstructure scale (grain size) and/or to the nanometer scale (crystallite size).

To summarize, the different investigations conducted (TEM, XRD, density, chemical analysis) show that the MMC materials consist of a matrix of nickel polygonal grains with submicron size and Ni<sub>3</sub>P as reinforcement in the form of spherical particles with size in the sub-micrometer range, but significantly lower than that of Ni grains. Furthermore, all obtained composites have a residual porosity, which decreases when the grain size increases. All together, these parameters likely control the mechanical and magnetic properties of the as-obtained MMCs. However, our recent work [8] has shown that Ni grain size plays the key role to tune the as-properties.

Thus, all mechanical and magnetic properties of the as-obtained MMCs are discussed and tentatively correlated with the grain size of the matrix, namely, Ni. Furthermore, the influence of Ni<sub>3</sub>P or porosity on this general behavior is specified in each case.

Yield strength, maximum stress, and plastic strain are mainly driven by the grain size of Ni, which constitutes the matrix. Figure 8 reports the yield strength (maximum stress is not reported, as it behaves similarly) and the plastic strain as a function of grain size. Similar behaviors were observed for MMCs published in the work of [8]. As shown in Figure 8, yield stress increased when the grain size decreased. Conversely, the plastic strain increased when the grain size increased. An important crossover of the mechanical response of the MMCs appeared around 350 nm of Ni grain, which corresponded to a crystallite size of around 50 nm. It is interesting to note that this threshold value was also observed for MMC samples studied in the work of [8] (Figure S2).

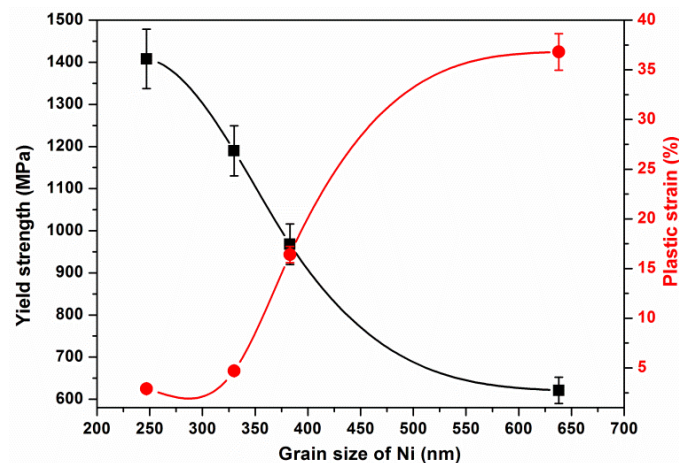


**Figure 8.** Variation of yield stress (■) and plastic strain (●) for the sintered samples as a function of the grain size of the Ni.

While the mechanical characteristics deduced from the compression tests do not depend on the porosity of the materials, Vickers hardness has a subtle behavior; it depends on the porosity in addition to the Ni grain size. It increases with the grain size to reach a maximum value for a grain size close to 380 nm, and then it decreases. Balancing porosity and Ni grain size makes it possible to obtain the highest hardness ( $p\%$  2.2, grain size 383 nm). The samples with a smaller grain size correspond to high porosities, which are harmful for obtaining high hardness. Beyond the critical size of 380 nm, the sample has a very low porosity, but it corresponds to an exaggerated growth of all nickel grains and Ni<sub>3</sub>P particles. This abnormal grain growth outweighed the increase in relative density, and hence explains the microhardness decrease.

The magnetic properties were also found to be closely related to the Ni grain size (Figure 9). The coercive field ( $H_c$ ) increased when the grain size decreased, similar to yield strength, while saturation magnetization values ( $M_s$ ) increased with the grain size in a manner similar to the plastic strain (curves corresponding to previous work [8] are shown in Figure S3). Like the mechanical behavior, a crossover behavior was observed around 350 nm of Ni grain size for the magnetic behavior of both sample series elaborated in the work of [8] and the present work. It is interesting to notice that this grain size corresponds to a crystallite size of around 50 nm, which is the critical crystallite size of the Ni magnetic mono-domain (Table 4) [31].

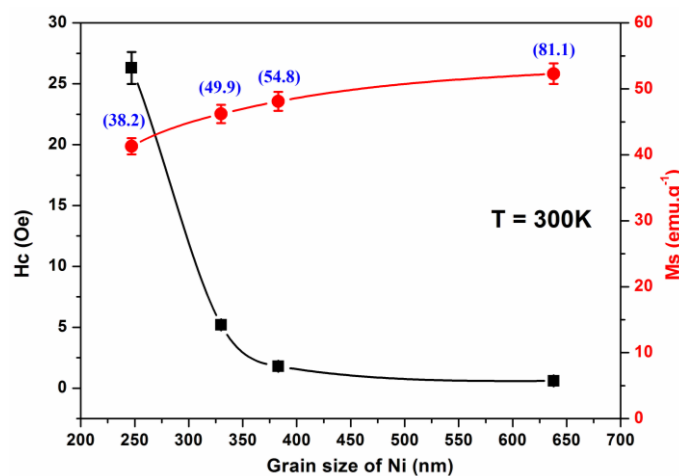


**Figure 9.** Variation of the saturation magnetization ( $M_s$ ) (●) and coercive field ( $H_c$ ) (■) at 300 K of the consolidated samples as a function of the grain size of the Ni. At each experimental point, we report, in blue parentheses, the crystallite size of Ni in nanometers.

All these results show that R-SPS is a useful sintering process to control the microstructure and physical properties of MMCs based on nickel. This can be achieved by following two different methods. The first one, developed in the work of [8], consists of varying the SPS conditions and starting from a given particle size. The second method (present work) consists of keeping identical SPS conditions and varying the size of the starting particles. Both processes led to MMCs with grain sizes varying in a wide range from 200 to 680 nm for Ni. This enables tuning the mechanical and magnetic properties on a large scale and opens the possibility of a crossover of these properties within the same composition only by controlling the growth of Ni grains.

In this work, together with the work of [8], we have shown that decreasing the grain size led to greater strength and a less ductile submicrometer grain-sized material in accordance with the Hall–Petch law [32,33]. This may be explained on the basis of dislocation density in the grains and subgrains (crystallites). Indeed, small grains contain few dislocations in comparison with large grains, inducing weaker stress at the grain boundary. Furthermore, decreasing the grain size leads to an increase of grain boundaries, which impedes the dislocation motion. In this case, the dislocation propagation in the adjacent grain needs a more important applied stress [34].

Finally, compared with the results published in the literature on pure nickel materials with comparable average sizes, we note that the yield strength, maximum stress, and microhardness are significantly higher [13,35] in our case. This result is mainly caused by the following:

- The presence of a secondary phase ( $\text{Ni}_3\text{P}$ ). Indeed, compared with single-phase samples with the same particle size, the presence of a secondary phase strengthens the microstructure and leads to higher values of microhardness and yield strengths [36,37].
- The difference in microstructure of these materials induced by the elaboration process. In the present study, the R-SPS process led to MMCs based on nickel with  $\text{Ni}_3\text{P}$  as a reinforcement starting from nanoparticles of Ni–P metastable alloys. The formation of  $\text{Ni}_3\text{P}$  occurred in situ by diffusion of P from the inside of the nanoparticles to their boundaries. This mechanism leads to strong chemical bonding between matrix and reinforcement components [38].

Decreasing the grain, and thus the crystallite size of the nickel, also affects the magnetic behavior. It leads to a higher coercive field ( $H_c$ ) and lower saturation magnetization ( $M_s$ ).

Because, as shown before, the grains of the as-obtained MMCs consisted of crystallites with sizes varying in the nanometer range (30–80 nm), it clearly appears that the magnetic behavior can be tentatively explained on the basis of interactions between these crystallites considered as magnetic nano-domains. The increase in  $H_c$  may be because of the change of the magnetization reversal mechanism in these nano-domains. When their size decreases, the crystallites are more magnetically close to mono-domains, and thus the magnetization reversal proceeds via a coherent rotation of the magnetic moment in each domain. This coherent mechanism needs a higher applied field [31] compared with the percolation process in a multi-domain magnetic state. Also, as soon as the crystallite size of the nickel approached the critical size of nickel (50 nm) (see Figure 8, blue numbers in parentheses), the coercive field of the MMC materials went abruptly to zero at RT (i.e., crossover-like behavior of the magnetic properties). This result allows us to speculate on the competition between the thermal instability of the magnetization moment into the mono-domain nanoparticles [31], causing the superparamagnetic behavior with the magnetic interactions between domains favoring the ferromagnetic properties. Our results show that approaching the critical size of the Ni crystallites drifts the thermal instability effect at higher temperatures than the RT one. Indeed, as shown in the inset of Figure 6b, when the crystallite size of the Ni matrix decreased below the critical size of Ni nanoparticles (i.e.,  $D_c = 50$  nm), the so-called blocking effect appeared at higher temperatures than the RT one. At RT, in fact, the hysteresis cycle went from a typical multi-domain magnetic behavior (NiP220SPS) to a soft ferromagnetic one (NiP50SPS). This allows the observation of soft ferromagnetic behavior for MMC systems presenting smaller Ni crystallite sizes than the critical one.

Unlike  $H_c$ ,  $M_s$  also depends on the presence of  $\text{Ni}_3\text{P}$  (a paramagnetic compound), which explains the slight decrease of  $M_s$  of all compounds of the series in comparison with bulk Ni. However, inside

this series, as for  $H_c$ , a regular variation was observed in the function of grain and crystallite sizes (i.e., when the grain and crystallite sizes decreased, the  $M_s$  decreased). Indeed, when the crystallite size decreased, the number of atoms at the surface increased. This led to an important number of disoriented moments in comparison with well-oriented moments inside of the crystallite. Such division into two magnetic sub-domains is responsible for the  $M_s$  decrease in comparison with the  $M_s$  of large particles, with the outside domain (surface domain) being considered a magnetic dead surface [39].

## 5. Conclusions

A bottom-up strategy combining a modified polyol process and the R-SPS process enabled us to elaborate MMCs based on Ni as a metal matrix and  $Ni_3P$  as a reinforcement phase. The modified polyol process led to Ni–P metastable alloy nanoparticles that were spherical in shape and had sizes between 50 and 220 nm. The heat treatment of the powder was performed by R-SPS for 10 min at 600 °C and 53 MPa. This transformed the starting metastable alloys into bulk submicrometer grain-sized MMCs, with Ni as the metal matrix and  $Ni_3P$  as the reinforcement. The metal matrix was formed by polygonal grains and the reinforcement phase appeared in the form of equiaxial nanoparticles. The polygonal grains were of sizes varying from 247 up to 638 nm, whereas the size of equiaxial particles varied in the range of 97–187 nm. TEM and X-ray diffraction analyses showed that the Ni grains were in fact constituted of crystallites, which can be considered as subgrains. Even more interesting was that the Ni grain size increased linearly with the crystallite size, which varied from 38 to 82 nm.

The presence of  $Ni_3P$  acted both on mechanical and magnetic properties: (i) as a reinforcement, it enhanced the strength of the as-elaborated MMCs; (ii) as a paramagnetic phase, it slightly reduced the  $M_s$  of the samples. However, it was clearly shown that the microstructure of the as-elaborated MMCs was the main factor driving their mechanical and magnetic behaviors. When the grain size decreased, the yield strength and coercive field ( $H_c$ ) increased. In contrast, strain to fracture (%) and saturation magnetization ( $M_s$ ) decreased when the grain size increased. It was observed that, for both properties, a crossover occurred at an Ni grain size of around 350 nm, corresponding to a crystallite size of 50 nm, which is the critical size of the Ni magnetic mono-domain. Below this grain size, the materials showed a relatively hard mechanical behavior (high strength) and semi-hard magnetic one ( $H_c$  around 100 Oe). For higher sizes, the materials evolved toward ductile and soft ferromagnetic magnetic behavior. Despite the nano-size of the crystallites considered as the magnetic mono-domains, the soft ferromagnetic behavior still existed at room temperature, which was likely owing to the magnetic interactions between the considered domains.

In summary, we have shown in this work that the mechanical and magnetic properties of MMCs based on Ni as a matrix and  $Ni_3P$  as a reinforcement can be easily tuned by controlling the grain and crystallite sizes of the Ni matrix. In turn, these sizes can be controlled by the size of Ni–P metastable alloy nanoparticles elaborated in polyol medium and transformed by R-SPS into MMCs under identical thermal heat conditions.

**Supplementary Materials:** The following are available online at <http://www.mdpi.com/2075-4701/10/1/112/s1>, Figure S1. TEM micrographs of the as-elaborated nickel-phosphorus precursor powder; grain size histogram; and percentage weight of phosphorus (a) NiP50, (b) NiP100, (c) NiP130, and (d) NiP220; Figure S2: Variation of yield stress and plastic strain of the consolidated samples at 600 °C from Ni–P powder (100 nm) versus the grain size of the Ni; Figure S3: Variation of the saturation magnetization ( $M_s$ ) and coercive field ( $H_c$ ) at 300 K of the consolidated samples at 600 °C from Ni–P powder (100 nm) versus the grain size of the Ni.

**Author Contributions:** M.A.B., S.M., F.S., and N.J. conceived and designed the experiments, M.A.B., S.M., and F.S. performed the experiments and analyzed the data. M.A.B. wrote the original draft. M.A.B., S.M., and N.J. wrote and edited the paper. N.J. supervised the work. All authors have read and agreed to the published version of the manuscript.

**Funding:** This research received no external funding.

**Acknowledgments:** Our thanks to Smiri, L.S. for her contribution in leading the thesis of M.A.B., whose current work is an extension.

**Conflicts of Interest:** The authors declare no conflict of interest.

## References

1. Anselmi-Tamburini, U.; Garay, J.E.; Munir, Z.A. Fast low-temperature consolidation of bulk nanometric ceramic materials. *Scripta Mater.* **2006**, *54*, 823–828. [[CrossRef](#)]
2. Cabouro, G.; Le Gallet, S.; Chevalier, S.; Gaffet, E.; Grin, Y.; Bernard, F. Dense  $\text{Mosi}_2$  produced by reactive flash sintering: Control of Mo/Si agglomerates prepared by high-energy ball milling. *Powder Technol.* **2011**, *208*, 526–531. [[CrossRef](#)]
3. Orrù, R.; Cao, G. Comparison of Reactive and Non-Reactive Spark Plasma Sintering Routes for the Fabrication of Monolithic and Composite Ultra High Temperature Ceramics (UHTC) Materials. *Materials* **2013**, *6*, 1566. [[CrossRef](#)] [[PubMed](#)]
4. Zhang, Y.; Zhang, J. Rapid reactive synthesis and sintering of textured  $\text{Ca}_3\text{Co}_4\text{O}_9$  ceramics by spark plasma sintering. *J. Mater. Process. Tech.* **2008**, *208*, 70–74. [[CrossRef](#)]
5. Turki, F.; Abderrazak, H.; Schoenstein, F.; Abdellaoui, M.; Jouini, N. SPS parameters influence on  $\text{Ti}_3\text{SiC}_2$  formation from Si/TiC: Mechanical properties of the bulk materials. *J. Alloys Compd.* **2017**, *708*, 123–133. [[CrossRef](#)]
6. Patisier, A.; Paul-Boncour, V. Fast synthesis of  $\text{LaFe}_{13-x}\text{Si}_x$  magnetocaloric compounds by reactive Spark Plasma Sintering. *J. Alloys Compd.* **2015**, *645*, 143–150. [[CrossRef](#)]
7. Bousnina, M.A.; Schoenstein, F.; Smiri, L.S.; Jouini, N. Facile synthesis of metastable Ni–P nanostructured materials by a novel bottom-up strategy. *Solid State Sci.* **2015**, *40*, 13–19. [[CrossRef](#)]
8. Bousnina, M.A.; Turki, F.; Schoenstein, F.; Têtard, F.; Rabu, P.; Smiri, L.S.; Jouini, N. Bulk nanostructured NiP alloys: Elaboration from metastable NiP nanoparticles by spark plasma sintering; mechanical and magnetic properties. *J. Alloys Compd.* **2016**, *686*, 252–266. [[CrossRef](#)]
9. Dakhlaoui-Omrani, A.; Bousnina, M.A.; Smiri, L.S.; Taibi, M.; Leone, P.; Schoenstein, F.; Jouini, N. Elaboration of nickel nanoparticles by modified polyol process and their spark plasma sintering, characterization and magnetic properties of the nanoparticles and the dense nano-structured material. *Mater. Chem. Phys.* **2010**, *123*, 821–828. [[CrossRef](#)]
10. Roisnel, T.; Rodríguez-Carvajal, J. WinPLOTR: A Windows tool for powder diffraction patterns analysis. *Mater. Sci. Forum* **2001**, *378*, 118–123, [www.cdifx.univ-rennes1.fr/winplotr/winplotr.htm](http://www.cdifx.univ-rennes1.fr/winplotr/winplotr.htm). [[CrossRef](#)]
11. Rietveld, H. A profile refinement method for nuclear and magnetic structures. *J. Appl. Cryst.* **1969**, *2*, 65–71. [[CrossRef](#)]
12. Schmetterer, C.; Vizdal, J.; Ipser, H. A new investigation of the system Ni–P. *Intermetallics* **2009**, *17*, 826–834. [[CrossRef](#)]
13. Bui, Q.H.; Dirras, G.; Ramtani, S.; Gubicza, J. On the strengthening behavior of ultrafine-grained nickel processed from nanopowders. *Mater. Sci. Eng. A* **2010**, *527*, 3227–3235. [[CrossRef](#)]
14. Gubicza, J.; Bui, H.Q.; Fellah, F.; Dirras, G.F. Microstructure and mechanical behavior of ultrafine-grained Ni processed by different powder metallurgy methods. *J. Mater. Res.* **2009**, *24*, 217–226. [[CrossRef](#)]
15. Prasad, M.J.N.V.; Chokshi, A.H. Microstructural stability and superplasticity in an electrodeposited nanocrystalline Ni–P alloy. *Acta Mater.* **2011**, *59*, 4055–4067. [[CrossRef](#)]
16. Weil, L.; Marfouré, S. Variation thermique du champ coercitif du nickel aggloméré. *J. Phys. Radium* **1947**, *8*, 358–361. [[CrossRef](#)]
17. Ni, X.; Zhao, Q.; Zheng, H.; Li, B.; Song, J.; Zhang, D.; Zhang, X. A Novel Chemical Reduction Route towards the Synthesis of Crystalline Nickel Nanoflowers from a Mixed Source. *Eur. J. Inorg. Chem.* **2005**, *223*, 4788–4793. [[CrossRef](#)]
18. You, Y.; Gu, C.; Wang, X.; Tu, J. Electrochemical Synthesis and Characterization of Ni–P Alloy Coatings from Eutectic–Based Ionic Liquid. *J. Electrochem. Soc.* **2012**, *159*, D642–D648. [[CrossRef](#)]
19. Gu, C.; Lian, J.; Li, G.; Niu, L.; Jiang, Z. High corrosion-resistant Ni–P/Ni/Ni–P multilayer coatings on steel. *Surf. Coat. Tech.* **2005**, *197*, 61–67. [[CrossRef](#)]
20. Changgeng, X.; Xinmin, H.; Zonggang, D.; Yanwen, W. Properties of electroless Ni–P and Ni–P–SiC. *Plat. Surf. Finish.* **1989**, *76*, 90–93.
21. Keong, K.G.; Sha, W.; Malinov, S. Hardness evolution of electroless nickel–phosphorus deposits with thermal processing. *Surf. Coat. Technol.* **2003**, *168*, 263–274. [[CrossRef](#)]
22. Guo, Z.; Keong, K.G.; Sha, W. Crystallisation and phase transformation behaviour of electroless nickel phosphorus platings during continuous heating. *J. Alloys Compd.* **2003**, *358*, 112–119. [[CrossRef](#)]

23. Deng, J.; Chen, H.; Bao, X.; Muhler, M. The effect of cyclic oxidation-reduction pretreatments on an amorphous Ni80P20 catalyst: An XPS/UPS/ISS study. *Appl. Surf. Sci.* **1994**, *81*, 341–346. [[CrossRef](#)]
24. Wang, Y.; Brogan, K.; Tung, S.C. Wear and scuffing characteristics of composite polymer and nickel/ceramic composite coated piston skirts against aluminum and cast iron cylinder bores. *Wear* **2001**, *250*, 706–717. [[CrossRef](#)]
25. Krishnan, K.H.; John, S.; Srinivasan, K.N.; Praveen, J.; Ganesan, M.; Kavimani, P.M. An overall aspect of electroless Ni-P depositions-A review article. *Metall. Mater. Trans. A* **2006**, *37*, 1917–1926. [[CrossRef](#)]
26. Bousnina, M.A.; Dakhlaoui-Omrani, A.; Schoenstein, F.; Madec, P.; Haddadi, H.; Smiri, L.S.; Jouini, N. Spark plasma sintering and hot isostatic pressing of nickel nanopowders elaborated by a modified polyol process and their microstructure, magnetic and mechanical characterization. *J. Alloys Compd.* **2010**, *504*, S323–S327. [[CrossRef](#)]
27. Panagopoulos, C.N.; Papachristos, V.D.; Sigalas, C. Tensile behaviour of as deposited and heat-treated electroless Ni-P deposits. *J. Mater. Sci.* **1999**, *34*, 2587–2600. [[CrossRef](#)]
28. Deng, J.-F.; Li, H.; Wang, W. Progress in design of new amorphous alloy catalysts. *Catal. Today* **1999**, *51*, 113–125. [[CrossRef](#)]
29. Gubicza, J.; Nauyoks, S.; Balogh, L.; Labar, J.; Zerda, T.W.; Ungár, T. Influence of sintering temperature and pressure on crystallite size and lattice defect structure in nanocrystalline SiC. *J. Mater. Res.* **2007**, *22*, 1314–1321. [[CrossRef](#)]
30. Kvackaj, T.; Kovacova, A.; Kocisko, R.; Bidulska, J.; Lityńska-Dobrzyńska, L.; Jenei, P.; Gubicza, J. Microstructure evolution and mechanical performance of copper processed by equal channel angular rolling. *Mater. Charact.* **2017**, *134*, 246–252. [[CrossRef](#)]
31. Leslie-Pelecky, D.L.; Rieke, R.D. Magnetic Properties of Nanostructured Materials. *Chem. Mater.* **1996**, *8*, 1770–1783. [[CrossRef](#)]
32. Hall, E.O. The Deformation and Ageing of Mild Steel: III Discussion of Results. *Proc. Phys. Soc. B* **1951**, *64*, 747–753. [[CrossRef](#)]
33. Petch, N.J. The Cleavage Strength of Polycrystals. *J. Iron Steel Inst.* **1953**, *174*, 25–28.
34. Carlton, C.E.; Ferreira, P.J. What is behind the inverse Hall–Petch effect in nanocrystalline materials? *Acta Mater.* **2007**, *55*, 3749–3756. [[CrossRef](#)]
35. Krasilnikov, N.; Lojkowski, W.; Pakiel, Z.; Valiev, R. Tensile strength and ductility of ultra-fine-grained nickel processed by severe plastic deformation. *Mater. Sci. Eng. A* **2005**, *397*, 330–337. [[CrossRef](#)]
36. Saboori, A.; Dadkhah, M.; Fino, P.; Pavese, M. An Overview of Metal Matrix Nanocomposites Reinforced with Graphene Nanoplatelets: Mechanical, Electrical and Thermophysical Properties. *Metals* **2018**, *8*, 423. [[CrossRef](#)]
37. Ferguson, J.B.; Sheykh-Jaberi, F.; Kim, C.-S.; Rohatgi, P.K.; Cho, K. On the strength and strain to failure in particle-reinforced magnesium metal-matrix nanocomposites (Mg MMNCs). *Mater. Sci. Eng. A* **2012**, *558*, 193–204. [[CrossRef](#)]
38. Chu, K.; Liu, Z.; Jia, C.; Chen, H.; Liang, X.; Gao, W.; Tian, W.; Guo, H. Thermal conductivity of SPS consolidated Cu/diamond composites with Cr-coated diamond particles. *J. Alloys Compd.* **2010**, *490*, 453–458. [[CrossRef](#)]
39. Zheng, M.; Wu, X.C.; Zou, B.S.; Wang, Y.J. Magnetic properties of nanosized MnFe<sub>2</sub>O<sub>4</sub> particles. *J. Magn. Magn. Mater.* **1998**, *183*, 152–156. [[CrossRef](#)]

